J. Fluid Mech. (2025), *vol.* 1007, R6, doi:10.1017/jfm.2025.152

On the size of transitional boundary-layer streaks

José M. Faúndez Alarcón[1], **Ardeshir Hanifi**[1] **and Dan S. Henningson**[1]

[1]FLOW, Department of Engineering Mechanics, KTH Royal Institute of Technology, SE-10044 Stockholm, Sweden

Corresponding author: José M. Faúndez Alarcón, josfa@kth.se

(Received 29 October 2024; revised 24 January 2025; accepted 26 January 2025)

A collection of secondary instability calculations in streaky boundary layers is presented. The data are retrieved from well-resolved numerical simulations of boundary layers forced by free-stream turbulence (FST), considering different geometries and FST conditions. The stability calculations are performed before streak breakdown, taking place at various Rey_x the Reynolds number based on the streamwise coordinate. Despite the rich streak population of various sizes, it is found that breaking streaks have similar aspect ratios, independently of the streamwise position where they appear. This suggests that wider streaks will break down further downstream than thinner ones, making the appearance of secondary instabilities somewhat independent of the streak's wavelength. Moreover, the large difference in the integral length scale among the simulations suggests that this aspect ratio is also independent of the FST scales. An explanation for this behaviour is provided by showing that these breaking streaks are in the range of perturbations that can experience maximum transient growth according to optimal disturbance theory. This could explain why, at a given streamwise position, there is a narrow spanwise wavelength range where streak breakdown is more likely to occur.

Key words: boundary layer receptivity, boundary layer stability, transition to turbulence

1. Introduction and background

Free-stream turbulence (FST) induced transition is one of the many routes to turbulence that can take place in a boundary layer. Due to its relevance in engineering applications, there has been produced abundant work in the topic. From all these investigations, we have a general good understanding of the process and steps involved in this scenario. This route to transition is initiated with the receptivity of free-stream disturbances which can be of linear or nonlinear nature (Brandt *et al.* 2002), followed by the formation and amplification of streaks due to the lift-up effect (Landahl 1980). The emergence of

secondary instabilities causes the final streak breakdown, resulting in the nucleation of turbulent spots (Schlatter *et al.* 2008) and the subsequent fully turbulent boundary layer. For the interested reader, a more detailed description of the whole process can be found, for instance, in Matsubara & Alfredsson (2001); Brandt *et al.* (2004); Zaki (2013).

In spite of the numerous experimental and numerical available evidence at our disposal, there are still some details that remain elusive. This is generally attributed to the dependence not only on the specific boundary conditions for each case dictating the stationary base flow, but also on the characteristics of the imposed FST. The latter is commonly defined from its turbulence intensity Tu and an integral length scale L_{11}, which is obtained from two-point correlation measurements and that determines how energy is distributed along the broadband FST spectrum. From an application perspective, probably the most interesting quantity is the streamwise position where transition to turbulence will take place under certain conditions. While the effect of Tu is well understood, the same is not true for L_{11}. Notably, Fransson & Shahinfar (2020) showed in the same experimental campaign that depending on the Tu level, decreasing L_{11} can promote or delay transition, which goes against the general trend observed in previous investigations where only delay was observed (see, for instance, Brandt *et al.* 2004; Jonáš *et al.* 2000). This result motivated the work by Durović *et al.* (2024), where an advance in transition was observed in a numerical simulation.

The results for a zero pressure gradient (ZPG) flat plate in Fransson & Shahinfar (2020) led to the hypothesis that an optimal ratio between L_{11} and the boundary-layer thickness at transition position $\delta_{tr} = \sqrt{\nu x_{tr}/U_\infty}$ must exist, with ν the kinematic viscosity and U_∞ the free-stream velocity. This ratio should be optimal in the sense that transition happens closest to the leading edge for a fixed turbulence intensity. One drawback on the use of this parameter is that it includes the streamwise position x_{tr} where transition takes place, which is actually the quantity we are searching for. Nevertheless, this problem can be seen as finding the optimal L_{11} such that unstable/breaking streaks arise closest to the leading edge.

The stability of streaks, and the resultant appearance of secondary instabilities, has been generally associated with their amplitude (Andersson *et al.* 2001), where optimal disturbance theory (Andersson *et al.* 1999; Luchini 2000) gives us the most likely waves due to their maximum amplification. However, it has also been proposed that the amplitude might not be the only relevant parameter to discriminate between stable and unstable streaks. For instance, the discrimination based on a neural network by Hack & Zaki (2016) suggests that other quantities such as the wall-normal velocity, streamwise momentum and the spanwise shear can be valuable parameters to take into account for the identification of breaking streaks.

One stage of FST induced transition that is not always easy to account for is receptivity, setting the scale and initial amplitude of the disturbances inside the boundary layer. In this regard, a linear and a nonlinear mechanism have been proposed (Brandt *et al.* 2002). The linear mechanism is characterised by the direct penetration of free-stream vortices into the boundary layer, taking place close to the leading edge. On the other hand, the nonlinear mechanism can occur along the whole boundary layer through triad interactions. In the work by Durović *et al.* (2024), this latter mechanism was proposed as being responsible for turbulent spot inception. The reason being that the observed breaking streaks had a relative short spanwise wavelength, and those scales were not energetic close to the leading edge. This energy transfer can be explained by the preferred energy propagation towards higher spanwise wavenumbers (short wavelengths) through the β-cascade proposed by Henningson *et al.* (1993).

The purpose of the present work is to document different simulations of FST induced transition performed within our group where we have observed that secondary instabilities,

and therefore their hosting streaks, have a similar spanwise extension in their local boundary-layer scaling. Here, we also include some examples found in the literature. Further evidence that breaking streaks generally reach a certain aspect ratio condition can also be found in the work by Hack & Zaki (2016), where they showed that for different pressure gradients, the shapes of breaking streaks were almost identical when scaled by the momentum thickness at transition position. By analysing the perturbations' optimal growth, we see that the width of the breaking streaks are in the range of those reaching maximum amplification.

The remainder of this paper is structured as follows. In § 2 we present the framework for stability analysis. Section 3 includes the list of cases with their corresponding unstable modes. And finally, in § 4 we expand on some concluding remarks.

2. Stability analysis

The stability of the flow fields is studied in the local framework on planes normal to the streamwise direction. These planes are taken directly from the direct numerical simulation (DNS) solutions upstream and at previous time steps of a turbulent spot nucleation. In this context, we decompose the velocity and pressure field as

$$\mathbf{Q}(t,\,x,\,y,\,z) = \mathbf{Q}_0(y,\,z;\,t,\,x) + \varepsilon\mathbf{q}(t,\,x,\,y,\,z), \tag{2.1}$$

with $\mathbf{x} = (x,\,y,\,z)^{\mathsf{T}}$ the streamwise, wall-normal and spanwise coordinates, $\mathbf{Q}_0 = (U,\,V,\,W,\,P)^T$ the DNS solution for the velocity vector $(U,\,V,\,W)^T$ along the corresponding coordinates and the pressure P, and ε the perturbation amplitude with corresponding shape $\mathbf{q} = (u,\,v,\,w,\,p)^{\mathsf{T}}$. For the perturbation function, we assume a normal mode in time and along the streamwise direction $\mathbf{q} = \hat{\mathbf{q}}(y,\,z)\exp(-i(\alpha x - \omega t))$, with α the streamwise wavenumber and ω a complex value whose real and imaginary parts represent the angular frequency and temporal growth rate, respectively. The use of a local temporal framework for the stability analysis is justified by the time-scale separation between the low-frequency streaks and their high-frequency secondary instabilities. Examples of similar procedures can be found, for instance, in Hack & Zaki (2014); Faúndez Alarcón *et al.* (2024*a*).

By substituting (2.1) in the Navier–Stokes equations and neglecting high-order terms we obtain the system

$$(\mathcal{C} - \Delta)\,\hat{u} + \left(\mathcal{D}_y U\right)\hat{v} + (\mathcal{D}_z U)\,\hat{w} + i\alpha\,\hat{p} = i\omega\hat{u}, \tag{2.2a}$$

$$\left(\mathcal{C} - \Delta + \mathcal{D}_y V\right)\hat{v} + (\mathcal{D}_z V)\,\hat{w} + \mathcal{D}_y\,\hat{p} = i\omega\hat{v}, \tag{2.2b}$$

$$\left(\mathcal{D}_y W\right)\hat{v} + (\mathcal{C} - \Delta + \mathcal{D}_z W)\,\hat{w} + \mathcal{D}_z\,\hat{p} = i\omega\hat{w}, \tag{2.2c}$$

$$i\alpha\hat{u} + \mathcal{D}_y\hat{v} + \mathcal{D}_z\hat{w} = 0, \tag{2.2d}$$

where $\mathcal{C} = Ui\alpha + V\mathcal{D}_y + W\mathcal{D}_z$, $\Delta = 1/Re(-\alpha^2 + \mathcal{D}_y^2 + \mathcal{D}_z^2)$, $\mathcal{D}_y = \partial/\partial y$ and $\mathcal{D}_z = \partial/\partial z$, where Re is the Reynolds number. The discrete differential operators are built with a 4th-order finite difference scheme, while non-slip is imposed at the wall, periodicity along the span, and zero velocity in the far field. The generalised eigenvalue problem (2.2) is solved with a shift-and-invert Arnoldi algorithm.

3. Results

We present a summary of the analysed cases in table 1. The simulations consider different geometries, with and without leading edge, solvers, FST conditions and transition positions. However, they all share the same typical features of bypass transition from the

Case	Geometry	LE	$Tu\%$	L_{11}	Re_{x_1}	Re_{θ_1}	Reference
1	ZPG	No	3.0	19.4	3.80×10^5	393	Sasaki et al. (2019)
2	ZPG	Yes	3.4	119.5	1.72×10^5	275	Durović et al. (2024)
3	ZPG	Yes	3.45	45.3	0.82×10^5	190	Durović et al. (2024)
4	NACA0008	Yes	2.5	45.9	1.02×10^5	181	Faúndez Alarcón et al. (2024*b*)
5	ZPG	No	3.0	6.9	1.47×10^5	255	Hack & Zaki (2014)
6	APG	No	3.0	7.0	1.03×10^5	242	Hack & Zaki (2014)

Table 1. List of the study cases. The LE column indicates if the simulation includes the leading edge. Here Tu and L_{11} represent the free-stream turbulence characteristics; Re_{x_1} and Re_{θ_1} correspond to the position where the stability calculations were performed.

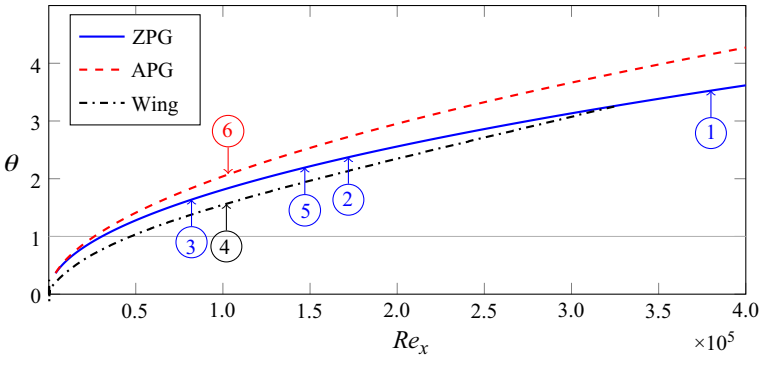

Figure 1. Momentum thickness θ of the three base flow configurations considered in this work. Here θ is made non-dimensional by the momentum thickness at $Re_\theta = 116$. The annotations indicate the case number and position where stability analysis was performed.

inception to streak breakdown. The FST conditions, Tu and L_{11}, correspond to those reported in the respective work at the leading edge/inflow. For better comparison, they have been made non-dimensional by the momentum thickness θ_0 at $Re_\theta = 116$, which only coincides with the inlet condition in Sasaki *et al.* (2019). Evidently, this means that the reported values in table 1 for Tu and L_{11} do not necessarily have those values at $Re_\theta = 116$ due to turbulence decay. The columns corresponding to Re_{x_1} and Re_{θ_1} in table 1 represent the position where the stability analysis was performed for the corresponding simulation. Besides of the differences between cases, it is worth emphasising that these planes were taken upstream and at previous time steps from turbulent spot nucleations. The nucleation events were identified from flow inspection and laminar–turbulent discrimination of the fields, following the procedure described in Faúndez Alarcón *et al.* (2024*a*).

To better visualise the different positions where the secondary instabilities emerge, figure 1 shows the momentum thickness and streamwise location for all the cases presented in table 1. Given that the stability calculations were performed in the still laminar flow, the momentum thickness,

$$\theta(x) = \int_0^\infty \left(1 - \frac{U(x,y)}{U_e(x)}\right) \frac{U(x,y)}{U_e(x)} \mathrm{d}y, \tag{3.1}$$

is obtained from the time-invariant base flow solution for the corresponding geometry, with $U_e(x)$ the free-stream velocity. The Hartree parameter for the adverse pressure

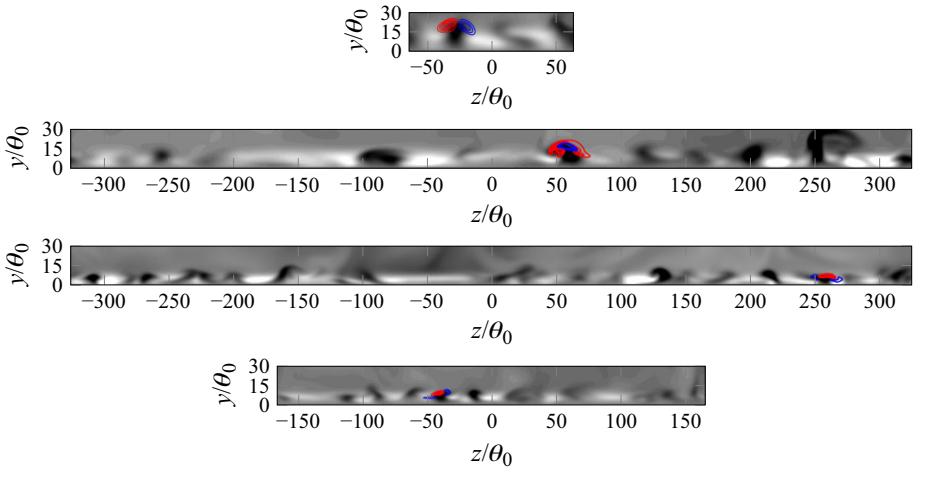

Figure 2. Planes where stability calculations were computed for cases 1 to 4 (top to bottom). The grey contours represent the streamwise velocity perturbations from −0.2 (black) to 0.2 (white), while the positive (red) and negative (blue) streamwise velocity components of the secondary instability are represented by the open contours. The axes are scaled by the momentum thickness at $Re_\theta = 116$.

gradient (APG) case is $\beta_H = -0.14$. We have chosen the momentum thickness as a scaling parameter because it has been shown that this scaling accounts for pressure gradient differences in algebraic growth (Corbett & Bottaro 2000).

Local stability analysis, described in § 2, was performed for cases 1–4, and the planes under consideration are presented in figure 2. Here, the axes have been normalised by the momentum thickness at $Re_\theta = 116$, making more clear the spanwise extension difference among the cases and the presence of streaks of various scales. The unstable modes shown in these planes were selected based on the fact that they preceded the nucleation of turbulent spots downstream and at a later time. By comparing the size of these unstable streaks for the different cases, we can see that the actual streak width does not seem to play a significant role regarding stability, with instabilities appearing on streaks of varied sizes.

Zoomed views of the unstable modes are included in figure 3, which also includes two adaptions of plots from Hack & Zaki (2014) (cf. their figures 6 and 19). These two plots also show the unstable modes on top of the streamwise velocity perturbation from their DNS. The axes have been made non-dimensional by the local momentum thickness θ_1 and centred around the secondary instability for better comparison. It can be noted that most of the unstable modes are located on top of a low-speed streak, while only the APG case shows an unstable mode in the shear between a low- and high-speed streak (an inner mode in the terminology adopted in Hack & Zaki (2014)). Interestingly, they all exhibit a similar spanwise extension in their local scaling, which seems to be independent of the mode symmetry, either sinuous or varicose, and their streamwise position.

The spanwise extension of the secondary instabilities can be more clearly seen by computing the energy distribution along the span as

$$E(z) = \int_0^{y_{\max}} \hat{\mathbf{u}}^H \hat{\mathbf{u}} \mathrm{d}y, \tag{3.2}$$

with $\hat{\mathbf{u}} = (\hat{u}, \hat{v}, \hat{w})^\mathsf{T}$ and the superscript H representing the complex conjugate. The energy distribution for the modes in cases 1–4 are shown in figure 4(*a*), where the curves have

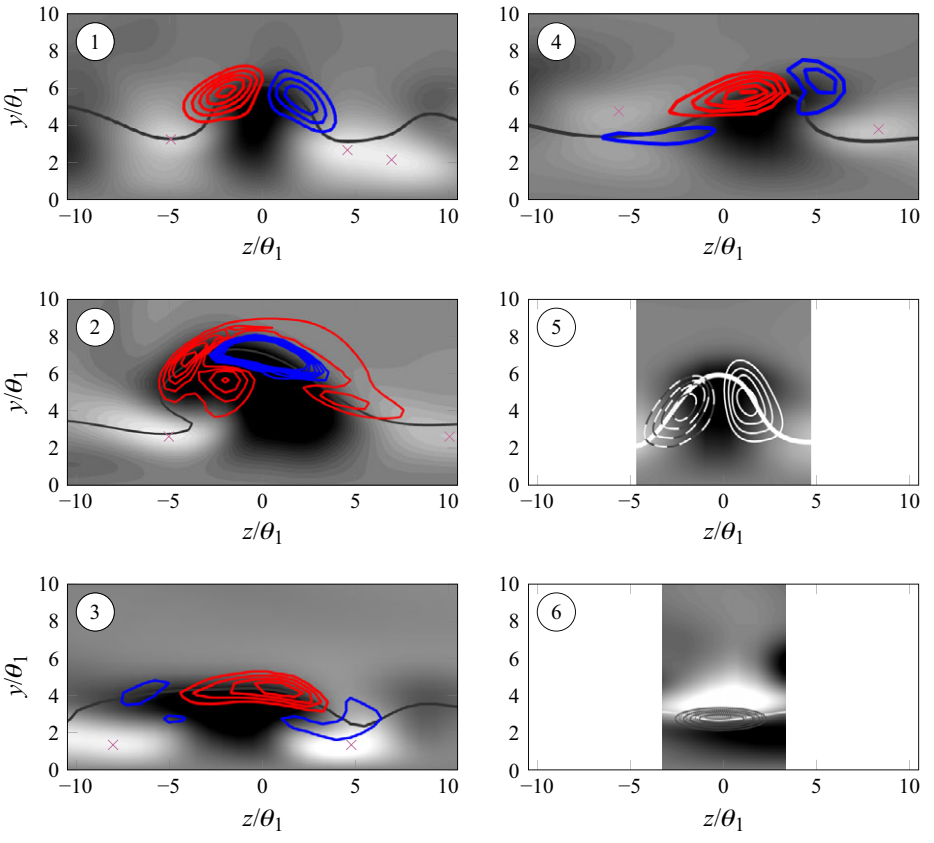

Figure 3. Zoomed view of the unstable modes with the axes scaled by the corresponding local momentum thickness θ_1. The colours for cases 1–4 are the same as in figure 2, with the grey solid line indicating the critical layer and the purple markers the perturbation local maxima. The plots for the unstable modes 5 and 6 have been adapted from Hack & Zaki (2014).

been normalised by their corresponding maximum along the span. From this figure, it can be seen that all of them have an extension in the range $\approx 8\theta(x)$–$14\theta(x)$. Statistical results are included in figure 4(*b*), showing the distribution of the spanwise width Δz of secondary instabilities normalised by the corresponding local momentum thickness. The stability calculations were performed in Faúndez Alarcón *et al.* (2024*a*), where the flow fields come from the same dataset as case 3 in the present manuscript. In particular, the distribution corresponds to instabilities reaching an N-factor $= 3$ and that were connected to nucleation events, with Δz based on the positions where $E(z)$ drops below 1 % of its maximum. Interestingly, most of the instabilities fall in a rather narrow range with a peak around $\approx 13\theta_1$. As a reference for the streak population range, figure 4(*b*) also includes the energy distribution of the streaky base flow in case 3 as a function of the spanwise wavelength, λ_z, at $y/\theta_1 = 3$. It is worth noting that there is some uncertainty on the streamwise position of the instability, since it corresponds to wave packets convected downstream appearing in a range of streamwise stations and a time window. Therefore, depending on the station where we perform the stability calculation, the scaling can vary slightly and so will the results shown in figure 4.

While the spanwise extension of the secondary instabilities could serve as a good indicator of the size of their hosting streaks, it is not necessarily the most accurate one.

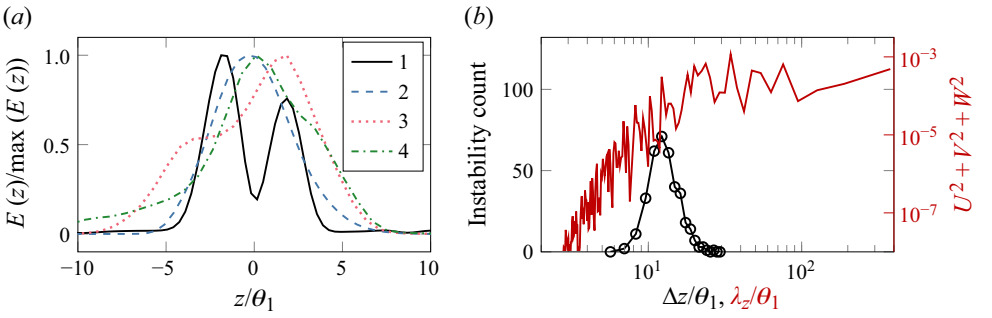

Figure 4. (*a*) Energy distribution of the unstable modes along the span. The curves correspond to the different cases and are centred at the corresponding modes' mean position. (*b*) The black markers show the distribution of instabilities from the same database as case 3. And, as a reference, the energy distribution of the streaky base flow of case 3 at $y/\theta_1 = 3$ is shown in red.

This is due mainly to secondary instabilities being localised on top of a distorted low-speed streak, which could lead to an underestimation of the unstable streak wavelength. An alternative approach is to find the local maxima of the streamwise velocity perturbation around the unstable streak, in order to identify the core of the contiguous high-speed streaks. This is shown with the markers on top of the flow fields in figure 3, and noting this is an approximated wavelength since the periodicity along z allows only for integer divisions of the domain's span. By taking the peak-to-peak length, we can estimate the streak wavelength, noting that they are all in the range $12-15\theta(x)$, which is, again, independent of the simulation conditions. Particularly, this prevailing spanwise wavelength does not change with the rather large L_{11} range.

One natural question that arises when analysing the streaks spacing is how they relate to those that can experience maximum amplification (Andersson *et al.* 1999; Luchini 2000). In this context, we compute the optimal energy gain at Re_{x_1} for stationary disturbances $\omega = 0$ starting at a prescribed initial position x_0 as

$$G(x_1, \beta) = \max_{\mathbf{u}_0} \frac{\int \mathbf{u}_1^H \mathbf{u}_1 \mathrm{d}y}{\int \mathbf{u}_0^H \mathbf{u}_0 \mathrm{d}y}, \tag{3.3}$$

where β is the spanwise wavenumber, and, in a slight abuse of notation, $\mathbf{u}$ corresponds to the perturbation with respect to the time-invariant base flow and not to the secondary instability. The calculations in this case were made non-dimensional by the streamwise position x_1. Figure 5 includes the optimal growth against the spanwise wavelength considering different x_0 for a Blasius boundary layer, the wing profile and, for completeness, it also includes the curves for APG and favourable pressure gradient (FPG) considering the Hartree parameter $\beta_H = -0.14$ and $\beta_H = 0.14$, respectively. Due to the Reynolds independence characteristic of the Blasius boundary layer for optimal growth (Andersson *et al.* 1999), the corresponding plot is valid for all ZPG cases under study. On the other hand, the optimal results for the wing are specific for this particular case and Re_{x_1}. The lines associated with $x_0 = 0.01$ can be directly contrasted against the results in Andersson *et al.* (1999) and Faúndez Alarcón *et al.* (2022), for Blasius and the wing boundary layer, respectively. These are related to linear receptivity mechanisms, where the perturbations penetrate the boundary layer close to the leading edge (Brandt *et al.* 2002) to then grow according to their optimal component. The interpretation of larger values of x_0 is less clear, but they can be related to nonlinearly generated perturbations in the boundary layer that will nonetheless grow due to linear mechanisms (Schmid & Henningson 2001).

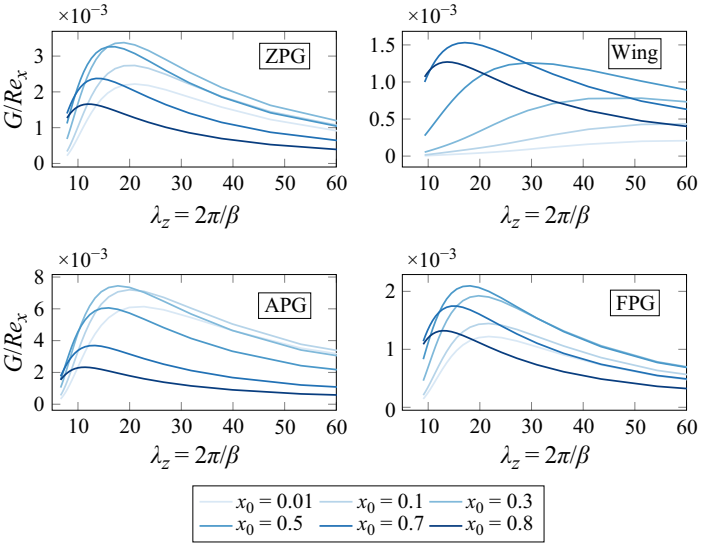

Figure 5. Optimal growth vs spanwise wavelength λ_z for different initial positions x_0. The wavelength has been made non-dimensional by the local momentum thickness at the objective position.

Interestingly, when optimal initial perturbations are placed closer to the objective position there is a shift towards shorter wavelengths that can reach higher amplification. This behaviour is much more pronounced in the optimal growth corresponding to the wing.

When comparing the results shown in figure 5 with the peak-to-peak spacing in figure 3, we can see that the breaking streaks are in the range of those reaching maximum amplification. In this type of transition scenario, with a broadband disturbance spectrum, the optimal amplification could explain why it is within this range that breaking streaks are more likely to be found. There is, of course, an intricate interplay between energy transfer and optimal growth that will set the streak spacing in the boundary layer, and which is largely dependent on the inflow FST conditions. While small spanwise wavenumbers (large wavelengths) will reach maximum amplification downstream in the boundary layer, the preferred energy propagation towards higher wavenumber through the β-cascade (Henningson *et al.* 1993) can give rise to shorter spanwise wavelength able to reach maximum amplification upstream, even when they were not initially present in the incoming FST. Unlike linear receptivity, the nonlinear interactions responsible for the energy transfer can take place throughout the boundary layer, profiting from the optimal growth that downstream induced perturbations can achieve, as shown in figure 5.

4. Concluding remarks

In this work, we have collected the stability analysis of streaky flows in boundary layers for six different numerical simulations. The main purpose of this survey is to provide numerical evidence from well-resolved simulations of bypass transition regarding the spanwise spacing of the streak secondary instabilities and their hosting streaks. We have observed that independently of the geometry, FST conditions and streamwise positions, the spacing of the breaking streaks is in a rather narrow range when scaled by the local momentum thickness. This is particularly remarkable after noting the large variation in the integral length scale among the cases. Although figure 4 provides statistical support for our main conclusion in one of the cases, it is reasonable to assume that it holds for the other

cases as well, in particular since the shape of the streaks, their streamwise development and the characteristics of their secondary instability is the same in all cases.

We provide a plausible explanation for the seeming preference of a specific wavelength for breaking streaks. Through optimal disturbance theory, we show that this spanwise wavelength of $12-15\theta(x)$ is within the range of streaks that can reach maximum amplification. The question regarding the causality of optimal amplification on streak instabilities remains open, since the latter might respond to various streak properties other than only their amplitude, as suggested, for instance, by Hack & Zaki (2016). However, the fact that maximum transient growth is achieved within this range could explain, at least, why streaks around this width are more likely to be seen breaking down.

The emergence of breaking streaks with a specific wavelength due to their optimal growth could serve as a basis for the hypothesis posed by Fransson & Shahinfar (2020) about the existence of an optimal ratio between L_{11} and boundary-layer thickness at transition. By recognising the role of L_{11} in distributing the energy along the spectrum, it is then reasonable that there exists an optimal distribution such that the necessary streak amplification is achieved closest to the leading edge through their optimal growth. Such an optimisation problem, however, should consider not only the optimal growth but also the energy transfer taking place along the boundary layer.

The twofold effect of L_{11} observed experimentally by Fransson & Shahinfar (2020) and corroborated numerically by Durović *et al.* (2024) is also consistent with the ideas shown here. The observation that increasing L_{11} could also delay transition can be understood by noting that a very low wavenumber will reach maximum amplification farther downstream. This would make their breakdown unlikely, where a more likely breakdown will take place due to energy transfer through the β-cascade to a higher wavenumber that can actually grow at upstream positions. The lower the initial wavenumber, the slower their amplification will be, and therefore the longer it will take for the nonlinearities to propagate energy.

Acknowledgments. The original authors of the various data sets used in this work are gratefully acknowledged. The computations were performed on resources provided by The National Academic Infrastructure for Supercomputing in Sweden (NAISS) at PDC and NSC.

Funding. This work was funded by Vinnova through the NFFP project LaFloDes (grant number 2019-05369); the European Research Council (grant agreement 694452-TRANSEP-ERC-2015-AdG); and the Swedish e-Science Research Centre (SeRC).

Declaration of interests. The authors report no conflict of interest.

References

Alarcón, F., José, M., Cavalieri, A.V.G., Hanifi, A. & Henningson, D.S. 2024*a* Role of streak secondary instabilities on free-stream turbulence-induced transition. *J. Fluid Mech.* **988**, A6.

Alarcón, F., José, M., Hanifi, A. & Henningson, D.S. 2024*b* Numerical studies of bypass transition delay on a wing using optimal control theory. PhD Thesis, *Numerical Investigations of Bypass Transition and Its Control*. KTH Royal Institute of Technology.

Alarcón, F., José, M., Morra, P., Hanifi, A. & Henningson, D.S. 2022 Disturbance growth on a NACA0008 wing subjected to free stream turbulence. *J. Fluid Mech.* **944**, A44.

Andersson, P., Berggren, M. & Henningson, D.S. 1999 Optimal disturbances and bypass transition in boundary layers. *Phys. Fluids* **11** (1), 134–150.

Andersson, P., Brandt, L., Bottaro, A. & Henningson, D.S. 2001 On the breakdown of boundary layer streaks. *J. Fluid Mech.* **428**, 29–60.

Brandt, L., Henningson, D.S. & Ponziani, D. 2002 Weakly nonlinear analysis of boundary layer receptivity to free-stream disturbances. *Phys. Fluids* **14** (4), 1426–1441.

Brandt, L., Schlatter, P. & Henningson, D.S. 2004 Transition in boundary layers subject to free-stream turbulence. *J. Fluid Mech.* **517**, 167–198.

CORBETT, P. & BOTTARO, A. 2000 Optimal perturbations for boundary layers subject to stream-wise pressure gradient. *Phys. Fluids* **12** (1), 120–130.

DUROVIĆ, K., HANIFI, A., SCHLATTER, P., SASAKI, K. & HENNINGSON, D.S. 2024 Direct numerical simulation of transition under free-stream turbulence and the influence of large integral length scales. *Phys. Fluids* **36** (7), 074105.

FRANSSON, J.H.M. & SHAHINFAR, S. 2020 On the effect of free-stream turbulence on boundary-layer transition. *J. Fluid Mech.* **899**, A23.

HACK, M.J.P. & ZAKI, T.A. 2014 Streak instabilities in boundary layers beneath free-stream turbulence. *J. Fluid Mech.* **741**, 280–315.

HACK, M.J.P. & ZAKI, T.A. 2016 Data-enabled prediction of streak breakdown in pressure-gradient boundary layers. *J. Fluid Mech.* **801**, 43–64.

HENNINGSON, D.S., LUNDBLADH, A. & JOHANSSON, A.V. 1993 A mechanism for bypass transition from localized disturbances in wall-bounded shear flows. *J. Fluid Mech.* **250** (1), 169–207.

JONÁŠ, P., MAZUR, O. & URUBA, V. 2000 On the receptivity of the by-pass transition to the length scale of the outer stream turbulence. *Eur. J. Mech. (B/Fluid)* **19** (5), 707–722.

LANDAHL, M.T. 1980 A note on an algebraic instability of inviscid parallel shear flows. *J. Fluid Mech.* **98** (2), 243–251.

LUCHINI, P. 2000 Reynolds-number-independent instability of the boundary layer over a flat surface: Optimal perturbations. *J. Fluid Mech.* **404**, 289–309.

MATSUBARA, M. & ALFREDSSON, P.H. 2001 Disturbance growth in boundary layers subjected to free-stream turbulence. *J. Fluid Mech.* **430**, 149–168.

SASAKI, K., MORRA, P., CAVALIERI, A.V.G., HANIFI, A. & HENNINGSON, D.S. 2019 On the role of actuation for the control of streaky structures in boundary layers. *J. Fluid Mech.* **883**, 1–33, arXiv: 1902.04923.

SCHLATTER, P., BRANDT, L., DE LANGE, H.C. & HENNINGSON, D.S. 2008 On streak breakdown in bypass transition. *Phys. Fluids* **20** (10), 101505.

SCHMID, P.J. & HENNINGSON, D.S. 2001 *Stability and Transition in Shear Flows*. Springer.

ZAKI, T.A. 2013 From streaks to spots and on to turbulence: exploring the dynamics of boundary layer transition. In *Flow, Turbulence and Combustion*, vol. **91**, pp. 451–473. Kluwer Academic Publishers.